IC/95/283

INTERNATIONAL CENTRE FOR THEORETICAL PHYSICS

MEASURING THE FRACTAL DIMENSION OF SEISMIC SOURCE THROUGH THE HIGH-FREQUENCY FALL-OFF OF SOURCE SPECTRA

Z.L. Wu

Y.T. Chen

and

S.G. Kim

INTERNATIONAL ATOMIC ENERGY AGENCY

UNITED NATIONS EDUCATIONAL, SCIENTIFIC AND CULTURAL ORGANIZATION

MIRAMARE-TRIESTE

IC/95/283

International Atomic Energy Agency
and
United Nations Educational Scientific and Cultural Organization
INTERNATIONAL CENTRE FOR THEORETICAL PHYSICS

MEASURING THE FRACTAL DIMENSION OF SEISMIC SOURCE THROUGH THE HIGH-FREQUENCY FALL-OFF OF SOURCE SPECTRA

Z.L. Wu[1]
International Centre for Theoretical Physics, Trieste, Italy,

Y.T. Chen
Institute of Geophysics, State Seismological Bureau,
Beijing 100081, People's Republic of China

and

S.G. Kim
The Seismological Institute, Hanyang University,
425-791 Ahnsan, Kyonggi-do, Korea.

MIRAMARE - TRIESTE
September 1995

[1]This is a result of a previous visit to ICTP for research on Seismic Source.
Permanent address: Institute of Geophysics, State Seismological Bureau, Beijing 100081, People's Republic of China.

Abstract

Using the Wigner-distribution estimation, the high-frequency fall-off of source spectra was estimated. The technique was applied to the analysis of the source spectra of the July 22, 1994, Vladivostok M6.4 deep-focus earthquake and that of the July 22, 1994, Northern Japan Sea M5.7 deep-focus earthquake. It is shown that the high-frequency fall-off of the source spectra of these two earthquakes may be characterized by two parts. Between the first corner frequency f_1 and the second corner frequency f_2, the high-frequency fall-off of the source spectra can be represented by $f^{-5.0}$; above f_2, the high-frequency fall-off can be represented by $f^{-1.1}$. In the perspective of the fractal geometry of earthquake source, it seems that the deep-focus earthquakes under consideration may be characterized as being composed of some 'subevents'. On the other hand, each subevent has its complex structure.

1 Introduction

In the characterization of earthquake sources, the high-frequency fall-off of source spectra is one of the most important measures describing the overall properties of the seismic source. The modelling and observation of the high-frequency behavior of earthquake sources can be traced back to as early as the 1970s (see, *e.g.*, Brune, 1970; Hanks, 1979), while the recent interest in this problem comes from the description of complex moment release in the perspective of fractal geometry (see, *e.g.*, Frankel, 1991). For instance, Frankel (1991) has shown that if the high-frequency behavior of the source spectra $\Omega(\omega)$ can be described by the high-frequency fall-off constant γ

$$\Omega(\omega) \sim M_0 \left(\frac{\omega}{\omega_0}\right)^{-\gamma} = M_0 \left(\frac{f}{f_0}\right)^{-\gamma} \qquad (1)$$

in which M_0 is the scalar seismic moment, $\omega = 2\pi f$ is the angular frequency, $\omega_0 = 2\pi f_0$ is

the corner frequency, and the speed of the propagation of the moment release is taken to be infinite (corresponding to the Brune model for the 'classical' limit), the high-frequency fall-off constant γ will be determined by the fractal dimension D of the complex moment release as

$$\gamma = 5 - 1.5D \tag{2}$$

In this way the fractal dimension of the complex moment release can be measured from the analysis of source spectra and then compared with the theoretical modelling of the seismic source.

In practical analysis, however, often it is not easy to retrieve the source spectra from the spectra of the seismic record. It is well known that the spectra of seismic record $U(\omega)$ can be represented as

$$U(\omega) = \Omega(\omega) I(\omega) P A(\omega) \tag{3}$$

where the first term on the right hand side is the source spectra, $I(\omega)$ describes the effect of recording instrument, P is the propagation operator, and $A(\omega)$ is the attenuation operator and can be represented by

$$A(\omega) = \exp\left(-\frac{\omega R}{2Qc}\right) \tag{4}$$

in which R is the distance between the source and the receiver, c is the velocity of seismic waves in the source region, and $Q = Q(\omega)$ is the quality factor along the path from the source to the station. As we have known in recent years, the Q value, as a description of the path attenuation, has two origins. One is the intrinsic attenuation caused by the inelasticity of the medium. The other is the apparent attenuation coming from the scattering of seismic waves on the inhomogeneities within the lithosphere (Wu and Aki, 1988).

With the development of broadband seismographs, the term $I(\omega)$ is becoming nearer and nearer to a constant within a wide frequency band. The seperation of the effect of source complexity from that of path attenuation thus becomes the main goal in the analysis of the spectra of braodband seismic records. To seperate the two terms, $\Omega(\omega)$ and $A(\omega)$, several approaches have been proposed and undertaken, each of which has its own advantages and limitations. For instance, if there happens to be a small earthquake with its location and focal mechnism near to the large earthquake, the seismogram of the small earthquake recorded by the same instrument may be treated as the empirical Green's function (Harzell, 1978). Dividing the spectra of the large earthquake by that of the smaller one, the slope of the high-frequency fall-off can be obtained (see, *e.g.*, Wu *et al.*, 1987). This method need not to consider the structure along the path, avoiding the difficulty in the calculation of Green's functions for 3-D inhomogeneous medium. On the other hand, however, in most cases, the requirement that the locations and focal mechnisms of the small earthquake and the large one be similar to each other can not be reached ideally, and the corner frequency of the small earthquake forms the limitation of the frequency band in which the high-frequency behavior of the large earthquake can be studied. As one of the approaches to retrieve the information of the source from digital seismic record, in our approach, we tried to consider some kinds of combination of the spectra of seismic record to eliminate the effect of path attenuation, so that the high-frequency fall-off of the source spectra can be obtained directly from the seismogram. For this purpose, we chose the Wigner-distribution estimation as the tool for the

analysis.

2 Measuring the High-frequency Fall-off of Source Spectra Using Wigner-Distribution estimation

2.1 The Wigner-distribution

For a given time dependent function $f(t)$ with its spectra being $F(\omega)$, the Wigner-distribution may be defined by

$$W_f(t,\omega)=\int_{-\infty}^{\infty}\exp(-i\omega\tau)f(t+\frac{\tau}{2})f^*(t-\frac{\tau}{2})d\tau \tag{5}$$

$$W_F(\omega,t)=\frac{1}{2\pi}\int_{-\infty}^{\infty}\exp(i\zeta t)F(\omega+\frac{\zeta}{2})F^*(\omega-\frac{\zeta}{2})d\zeta \tag{6}$$

where * denotes the complex conjugate. It can be proved that (Claasen and Mecklenbraeuker, 1980)

$$W_f(t,\omega)=W_F(\omega,t) \tag{7}$$

and

$$\mathrm{Im}\,[\ W_F(\omega,t)]\ =0 \tag{8}$$

As a useful tool for singal analysis, the Wigner-distribution has been widely used in various fields such as optics, accoustics, and electronics.

2.2 Measuring the High-frequency Fall-off of Source Spectra Using Wigner-Distribution Estimation

Consider the seismic record $u(t)$. Its spectra is written as $U(\omega)$. Taken the Wigner-distribution of $u(t)$, one has

$$W_f(t,\omega)=\int_{-\infty}^{\infty}\exp(-i\omega\tau)u(t+\frac{\tau}{2})u^*(t-\frac{\tau}{2})d\tau \tag{9}$$

$$W_F(\omega,t)=\frac{1}{2\pi}\int_{-\infty}^{\infty}\exp(i\zeta t)U(\omega+\frac{\zeta}{2})U^*(\omega-\frac{\zeta}{2})d\zeta \tag{10}$$

In the view of Fourier transform, it can be obtained from the above equations that

$$\begin{aligned}U(\omega+\tfrac{\zeta}{2})U^*(\omega-\tfrac{\zeta}{2}) &= \int_{-\infty}^{\infty}W_F(\omega,t)\exp(-i\zeta t)dt \\ &= \int_{-\infty}^{\infty}W_f(t,\omega)\exp(-i\zeta t)dt\end{aligned} \tag{11}$$

As we have mentioned above, $U(\omega)$ can be represented by

$$U(\omega)\propto\Omega(\omega)\exp(-\frac{\omega R}{2Qc}) \tag{12}$$

Therefore

$$U(\omega+\tfrac{\zeta}{2})U^*(\omega-\tfrac{\zeta}{2})\propto\Omega(\omega+\tfrac{\zeta}{2})\Omega^*(\omega-\tfrac{\zeta}{2})\exp(-\frac{\omega R}{Qc}) \tag{13}$$

and

$$\Omega(\omega+\frac{\zeta}{2})\Omega^*(\omega-\frac{\zeta}{2})\exp(-\frac{\omega R}{Qc}) = A\int_{-\infty}^{\infty} W_R(\omega,t)\exp(-i\zeta t)dt = A\int_{-\infty}^{\infty} W_I(t,\omega)\exp(-i\zeta t)dt \quad (14)$$

where A is a scaling constant.

For a real function $u(t)$, the spectra satisfies

$$U(\omega) = U^*(-\omega) \quad (15)$$

therefore

$$\Omega(\omega) = \Omega^*(-\omega) \quad (16)$$

For equation (14), letting $\omega \to 0$, one has

$$\Omega^2(\frac{\zeta}{2}) = A\int_{-\infty}^{\infty} W_I(t,\omega)\exp(-i\zeta t)dt\Big|_{\omega\to 0} \quad (17)$$

In this way the contribution of the Q-value is automatically eliminated, and the pure source spectra can be obtained.

In the calculation with digital data, it is impossible to let ω to be zero because the resolution Δf in frequency domain is controled by the length of the time window T

$$\Delta f = \frac{1}{T} \quad (18)$$

In practical data processing, usually one can choose a small frequency f_R as the 'reference frequency' and let $\omega \to 2\pi f_R$ to get the approximate estimation of $\Omega^2(\frac{\zeta}{2})$ in (17). In this case, for frequencies much larger than f_R, the approximation can be a good estimation of the source spectra. For low frequencies, on the other hand, the approximation may have uncertainties.

2.3 Test of the Algorithm

As a test of the algorithm, the near-source broadband acceleration data from one of the aftershocks of the 1985 Luquan, Yunnan, China earthquake was analysed. Shown in Figure 1a is the three-component accelerogram. The station is located approximately 5*km* to the north of the earthquake, so the EW component (the third channel in Figure 1a) can be regarded as the transversal component (Wu and Chen, 1995). The broadband seismogram was recorded using DCS-302 broadband digital accelerograph, with the sampling rate of 100 sps. The time window is taken as 2.56s (256 points), and the 'reference frequency' is taken as 1.0 *Hz*. As the frequency response of the instrument is flat within its working frequency band, and what we are interested in is the high-frequency fall-off rather than the scalar seismic moment, in the figures as well as the discussions thereafter, no instrument corrections and propagation corrections will be made. Accordingly the spectra plot uses relative value. The source

spectra obtained from Wigner-distibution estimation gives the high-frequency fall-off constant $\gamma \approx 3.0$, as shown in Figure 1b. This conclusion is consistent with the result obtained using empirical Green's functions (*e.g.*, Wang, 1990), implying that the algorithm works well in retrieving the high-frequency properties of the source spectra.

Figure 1a Broadband accelerogram from one of the aftershocks of the 1985 Luquan, Yunnan, China earthquake. In this study the EW component (the third channel in the figure) is chosen for the analysis. For details see Wu and Chen (1995).

Figure 1b Source spectra obtained using the technique of this study. In the figure vertical axis is the relative amplitude. As a comparison, the straight lines shown in the figure have the slope of -1.0, -2.0, and -3.0, indicating the high-frequency fall-off of f^{-1}, f^{-2}, and f^{-3}.

Comparing to other applications of the Wigner-distribution in signal analysis, this approach is not a real application of the Wigner-distribution. It is only a modified version of the Fourier transform. The advantages of the Wigner-distribution in analysing non-stationary time series have not been fully used in this algorithm. Moreover, price has been paid that if the frequency band of f_N is considered, only the information within the frequency band of $f_N/2$ can be obtained. Nevertheless, our approach, as one of the possible options dealing with the problem of source spectra, may be used at least as a reference to the result obtained by other methods. Noticing that the high-frequency contents of source spectra are resulted from the fact that a large earthquake is composed of many small earthquakes, to some extent, our approach might be regarded as an extension of the empirical Green's functions, in which the small event is provided by the earthquake itself.

3 High-frequency Fall-off of Source Spectra of Deep-focus Earthquakes from Wigner-Distribution Estimation

3.1 The High-frequency Fall-off of the Vladivostok Earthquake and the Northern Japan Sea Earthquake

The technique discussed above was used in analysing the digital velocity records from the July 22, 1994, Vladivostok deep-focus earthquake and the July 22, 1994, Northern Japan Sea deep-focus earthquake. Table 1 gives the parameters of the two deep-focus earthquakes. The station Guntan is located approximately in the centroid of Korean peninsula (Kim and Lee, 1995). The configuration of the station and the earthquakes has the advantage that the propagation path of the body waves can be simple enough to avoid the problem of reverbration. Also when considering the vertical component, equivalently the disturbances of the reflection and conversion can be merged into the scattering effect, and, as a good

approximation, the attenuation operator may be represented by equation (4). The length of the frequency window is taken as 512 points, and the 'reference frequency' is taken as 0.5 *Hz*.

Table 1 Parameters of earthquakes in this study

Earthquake	Date	Origin time (UTC)	Location Lat.	Lon.	Depth (km)	Magnitude
Vladivostok	07/22/1994	03:36:31.71	42.30	132.89	473.0	6.4
N. Japan Sea	07/22/1994	03:55:58.73	41.18	132.35	515.1	5.7

Shown in Figure 2a and 3a are the velocity seismograms of the two earthquakes. The recording seismograph is the DR-2000 digital seismograph, the frequency response of which is flat above 2 *Hz*. The sampling rate is 50sps. It is found that the seismograms are contaminated by other smaller earthquakes and/or disturbances (Kim and Lee, 1995). In the analysis, however, only the main events, indicated by their clear large arrivals, are selected for the computation. The vertical component consisting P waves (the upper trace in the figures) is chosen for the analysis.

Figure 2a Velocity seismogram from the Vladivostok earthquake. In the figure the arrival of P-wave from the main event is indicated. For details see Kim and Lee (1995).

Figure 2b Source spectra of the Vladivostock earthquake. In the figure vertical axis is the relative amplitude. Corner frequencies are also indicated in the figure. See text for detail.

Figure 3a Velocity seismogram from the Northern Japan Sea earthquake. In the figure the arrival of P-wave from the main event is indicated. For details see Kim and Lee (1995).

Figure 3b Source spectra of the Northern Japan Sea earthquake. In the figure vertical axis is the relative amplitude. Corner frequencies are also indicated in the figure. See text for detail.

Figure 2b shows the source spectra of the Vladivostok earthquake obtained using the technique discussed above. It may be seen from the figure that the high-frequency fall-off of the source spectra can be divided into two parts. Between 1.7 *Hz* and 3.0 *Hz*, the fall-off slope is shown to be approximately 5.0. Above 3.0 *Hz*, the slope becomes approximately 1.4. The Northern Japan Sea earthquake has similar characteristics, as shown in Figure 3b. Between 2.8 *Hz* and 5.0 *Hz*, the fall-off slope is shown to be approximately 5.0. Above 5.0

Hz, the slope becomes approximately 1.4.

3.2 Discussion: Complexity of the Source in the Perspective of Fractal Geometry

The mechanism of deep-focus earthquakes is different from that of shallow ones and is not quite clear at present. However, it is shown that for the deep-focus earthquakes in the region of Japan Sea and the Sea of Okhotsk, most of the deep-focus earthquakes can be modelled as a double-couple source (Fukao and Kikuchi, 1987; Zang *et al.*, 1992). Based on such fact, it was argued that the deep-focus earthquakes may be caused by the slab penetration into the mantle and has the properties similar to shear dislocation. At least in kinematics, some of the results for shallow earthquakes may be used to the understanding of the properties of deep-focus earthquakes.

As a kinematic approach, the discussions of Frankel (1991) on the relation between the fractal dimension of the seismic source and the high-frequency fall-off of the source spectra seems also valid to discuss the overall properties of deep-focus earthquakes. The common idea is that a large earthquake is composed of many small earthquakes with different sizes, no matter whether the earthquakes are shear dislocation or not. Further more, the distribution of the small events has some scale-invariant properties. When the moment release is measured with different scales, say, when one covers the earthquake source by certain grains with their size to be R, the number N of the grains containing non-zero moment release will be proportional to a power of R:

$$N(R) \propto R^{-D} \tag{19}$$

where D is the fractal dimension of the moment release. Frankel (1991) has discussed the relation between the high-frequency fall-off and the fractal dimension of the shear dislocation source and obtained that

$$\gamma = 5 - 1.5D$$

If this formula can also be used to discuss the deep-focus earthquakes in this study, there will be something of special interest to the medelling of the seismic source. In the perspective of the fractal geometry of the source, it may be seen that for the earthquakes in this study, the source spectra shows two levels of complexity of the source. Seen in 'middle' scale, the fractal dimension of the source is near to 0, corresponding to the situation that the whole earthquake source is composed of some 'point source' or 'subevents'. The 'subevents' has a sparse distribution. The average distance between the subevents determines the first corner frequency f_1. For the M6.4 earthquake, $f_1 \approx 1.7Hz$; for the M5.7 earthquake, $f_1 \approx 2.8Hz$. As we take a closer look inside the subevent, *i.e.*, seen from source spectra with frequencies higher than the second frequency f_2, the high-frequency fall-off of the source spectra indicates that $D \approx 2.4$ if the above equation is valid for the analysis. It seems that if the subevents may be described by a double couple, the image of such 'rupture' is more or less similar to the image of landscape. Considering the pressure in the mantle, one of the most possible mechanisms leading to such complex structure must be the inhomogeneities within the seismogenic region, which is possibly caused by the subduction process. The second corner frequency f_2 is 3.0 *Hz* for the M6.4 Vladivostok earthquake and 5.0 *Hz* for the M5.7 North Japan Sea earthquake, indicating the size of the 'subevents'.

For a more general case, the seismic moment tensor can be defined by

$$M_{ij} = \int_{V_0} m_{ij} dV \tag{20}$$

where the integration is over the source region V_0, and m_{ij} is the density of moment release and may be defined by

$$m_{ij} = c_{ijkl}\varepsilon^T_{kl} \tag{21}$$

in which $c_{ijkl}\varepsilon^T_{kl}$ is the stress glut caused by the stressless strain ε^T_{kl}. In the view of the general seimic moment tensor, it is not necessary to assume that the seismic source is a shear dislocation. In this case the scaling law of the scalar seismic moment may be written as

$$M_0 \propto R^{\beta - D} \tag{22}$$

where the R^{β} term indicates the size of the source, and the R^{-D} term indicates the number density of the moment release. Assuming that the moment release occurr almost simultaneously over the source volume V_0, *i.e.*, using the Brune model, the radiated energy seen in scale R will be

$$\begin{aligned} E(R) &\propto N(R)\Omega^2(\omega)\omega^2 \\ &\propto R^{2\beta - 2\gamma - 3D}\omega^{2-2\gamma} \end{aligned} \tag{23}$$

The scale invariance requires that

$$\gamma = \beta - \frac{3}{2}D \tag{24}$$

The general idea in this section is similar to that of Frankel (1991), although the expressions have some differences. In the view of general moment release, qualitatively the above discussion is still valid, although the values of the fractal dimension may be different. Seen from the source spectra, there seems to be a sparse distribution of 'subevents', and each 'subevent' itself is 'dense' and complex. Accordingly it can be deduced that the moment release is concentrated in some small regions over the source. Such regions are small comparing to the whole source and distribute in a sparse pattern. The overall size of the source is determined by the average distance between the 'subevents'. On the other hand, however, as a close insight into the moment-release-concentrated region, it may be found that such regions are complex. It should be noted that there are obviously many other reasonable explanations about the source spectra. Our explanation is only one of the plausible argues.

4. Conclusion and Discussion

Using the Wigner-distribution estimation, we tried to seperate the effect of source complexity from that of path attenuation. Assuming that the path attenuation can be modelled by a frequency-dependent $Q(\omega)$, the high-frequency fall-off of source spectra can be directly estimated by using the Wigner-distribution estimation of the seismic records. The test of the algorithm using near-source broadband data shows that the technique is effective to eliminate

the effect of path attenuation and retrieve the high-frequency fall-off of the source spectra.

The technique was applied to the analysis of the source spectra of the July 22, 1994, Vladivostok M6.4 deep-focus earthquake and that of the July 22, 1994, Northern Japan Sea M5.7 deep-focus earthquake. It is shown that the high-frequency fall-off of the source spectra of these two earthquakes may be characterized by two parts. Between the first corner frequency f_1 and the second corner frequency f_2, the high-frequency fall-off constant is near to 5.0, while above the second corner frequency f_2, the high-frequency fall-off constant is near to 1.4. For the M6.4 earthquake, $f_1 \approx 1.7Hz$, $f_2 \approx 3.0Hz$. For the M5.7 earthquake, $f_1 \approx 2.8Hz$, $f_2 \approx 5.0Hz$.

In the perspective of the fractal geometry of earthquake source, it seems that the deep-focus earthquakes under consideration may be characterized as being composed of some 'subevents'. The structure of the 'subevent', on the other hand, is complex. Obviously, there are other explanations about the source spectra. It is clear that more detailed studies on the source process of these earthquakes will provide useful constraints on the discussion.

Acknowledgements

This study was sponsored by the Joint Foundation of Seismological Sciences of China. The research was also partly financed by the STEPI of Korea and the Korean Ministry of Education. Acknowledgement is also due to Mr. F. C. Gao and Mr. S. Y. Mah for their help in the pre-processing of the data and Ms. D. M. Yang for helpful discussions.

References

Brune, J. N., 1970. Tectonic stress and the spectra of seismic shear waves from earthquakes. *J. Geophys. Res.*, **75**: 4887-5009.

Claasen, T. A. C. M. and Mecklenbraeuker, W. F. G., 1980. The Wigner distribution: a tool for time-frequency signal analysis. *Philips. J. Res.*, **35**: 217-389.

Fukao, V. and Kikuchi, M., 1987. Source retrieval for mantle earthquake by iterative deconvolution of long-period P waves. *Tectonophysics*, **144**: 249-269.

Frankel, A., 1991. High-frequency spectral fall off of earthquakes, fractal dimension of complex rupture, *b* value, and the scaling of strength on faults. *J. Geophys. Res.*, **96**: 6291-6332.

Hanks, T. C., 1979. *b* values and $\omega^{-\gamma}$ seismic source models: implications for tectonic stress variations along active crustal fault zones and the estimation of high-frequency strong ground motion. *J. Geophys. Res.*, **84**: 2235-2242.

Harzell, S. H., 1978. Earthquake aftershock as Green's function. *Geophys. Res. Lett*, **5**: 1-4.

Kim, S. G. and Lee, S. K., 1995. Determination of the hypocentral parameters outside the seismic array

using a single station of three-component. *The Journal of Engineering Geology*, 5: 59-74.

Wang, P. D., 1990. *Study of Near-source Strong Ground Motion*. Ph.D. thesis, the Institute of Geophysics, State Seismological Bureau, China, 120pp, in Chinese with English abstract.

Wu, F. T., Wang, P. D. and Chen, Y. T., 1987. Q_P and Q_S in Beijing and Jianchuan, Yunnan, China. *Acta Seismologica Sinica*, 9: 337-346, in Chinese with English abstract.

Wu, R.-S. and Aki, K. (*eds.*), 1988. *Scattering and Attenuation of Seismic Waves*, vol. I. Birkhaeuser Verlag, 447pp.

Wu, Z. L. and Chen, Y. T., 1995. Measuring the high-frequency fall-off of source spectra using the Wigner-distribution estimation. In: *Developments in Seismological Observation Technique and Space Sciences: In Honour of the 80th Birthday of Professor Qin Xinling*. Seismological Press, in Chinese with English abstract, to be published.

Zang, S. X., Wu, Z. L. and Ning, J. Y., 1992. Stress state and deep deformation of subduction zone in Japan Sea and the Sea of Okhotsk and the problem of slab penetration into the lower mantle. *Acta Geophysica Sinica*, 35: 560-573, in Chinese and English.

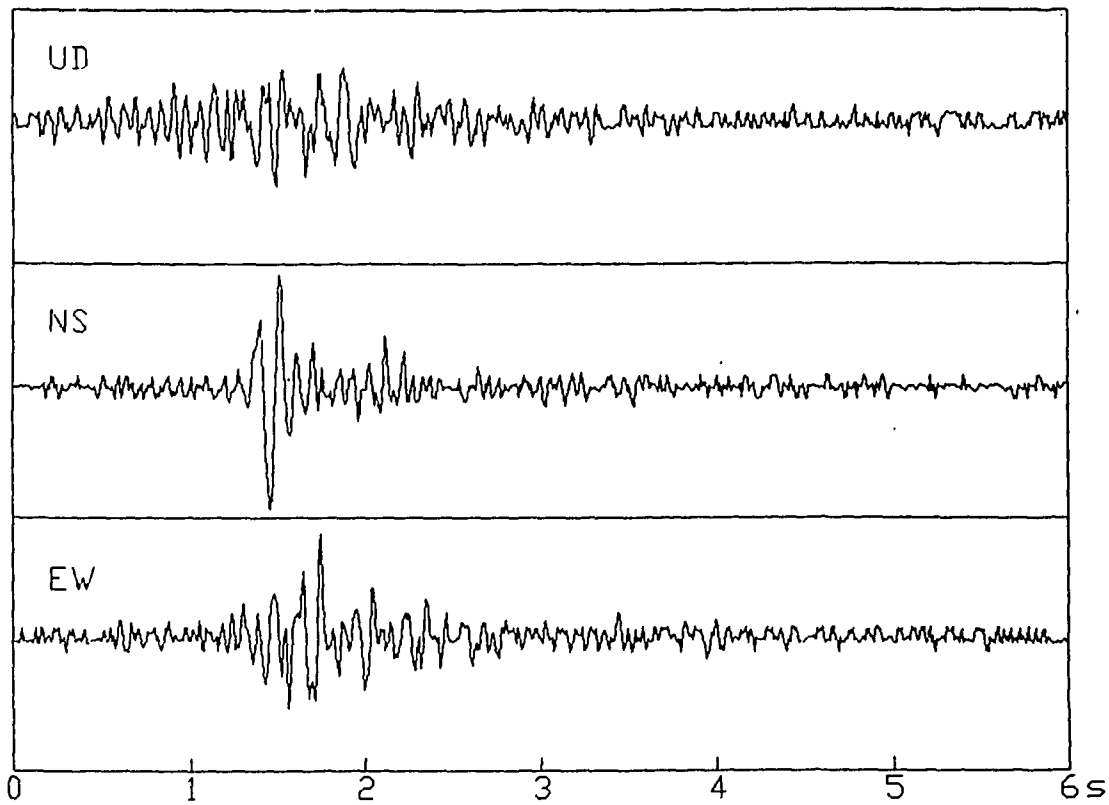

Fig.1a

Figure 1a Broadband accelerogram from one of the aftershocks of the 1985 Luquan, Yunnan, China earthquake. In this study the EW component (the third channel in the figure) is chosen for the analysis. For details see Wu and Chen (1995).

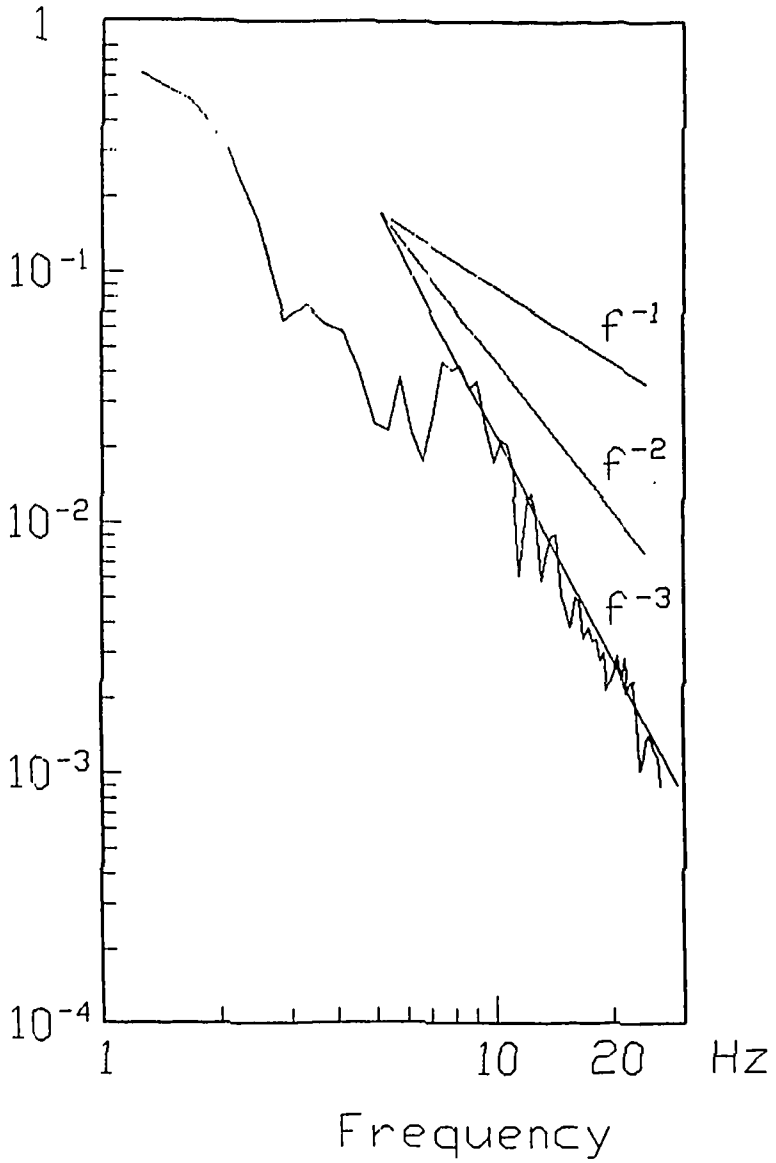

Fig.1b

Figure 1b Source spectra obtained using the technique of this study. In the figure vertical axis is the relative amplitude. As a comparison, the straight lines shown in the figure have the slope of -1.0, -2.0, and -3.0, indicating the high-frequency fall-off of f^{-1}, f^{-2}, and f^{-3}.

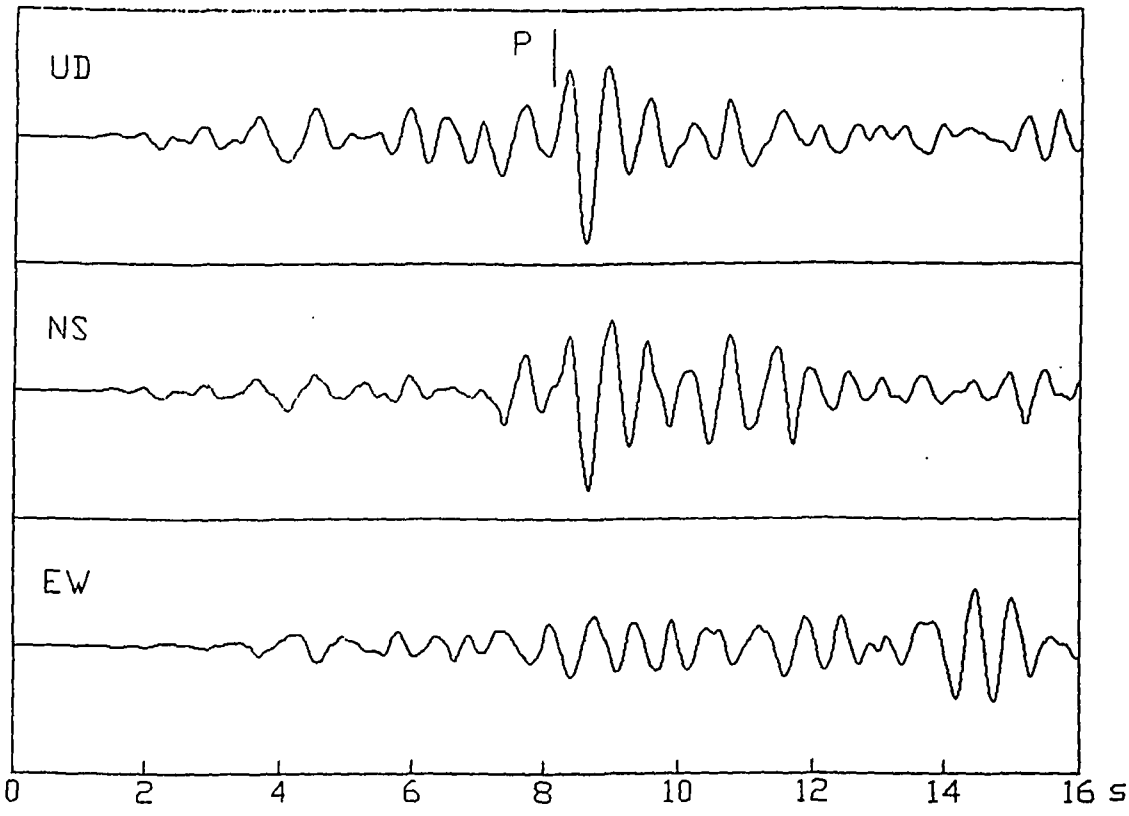

Fig.2a

Figure 2a Velocity seismogram from the Vladivostok earthquake. In the figure the arrival of P-wave from the main event is indicated. For details see Kim and Lee (1995).

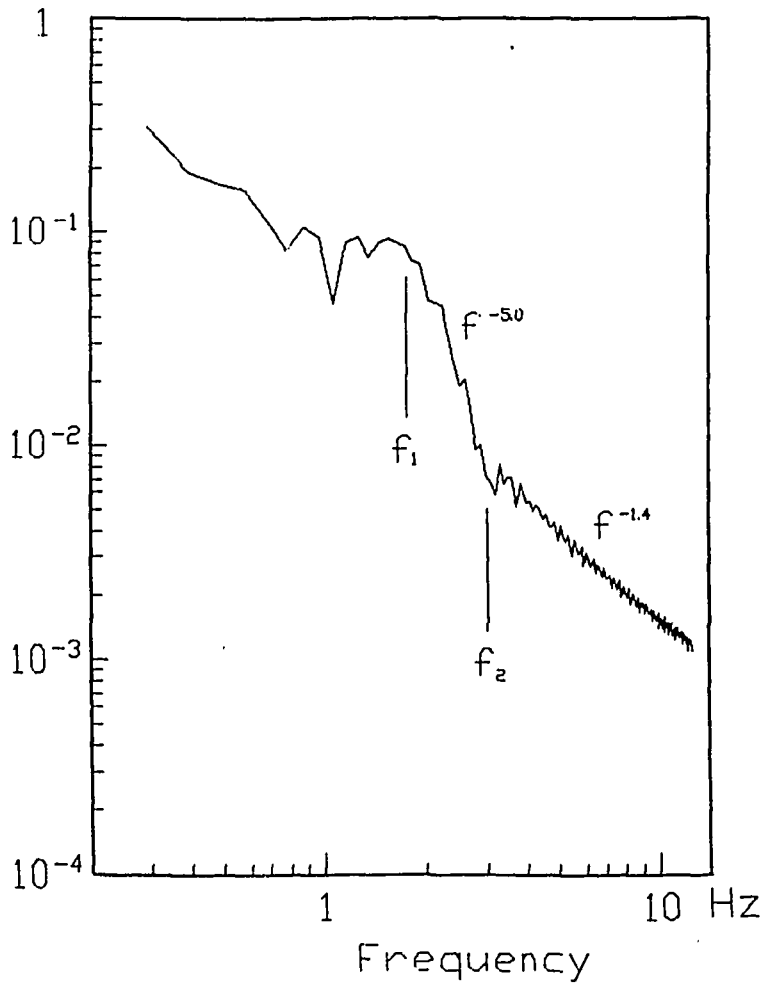

Fig.2b

Figure 2b Source spectra of the Vladivostock earthquake. In the figure vertical axis is the relative amplitude. Corner frequencies are also indicated in the figure. See text for detail.

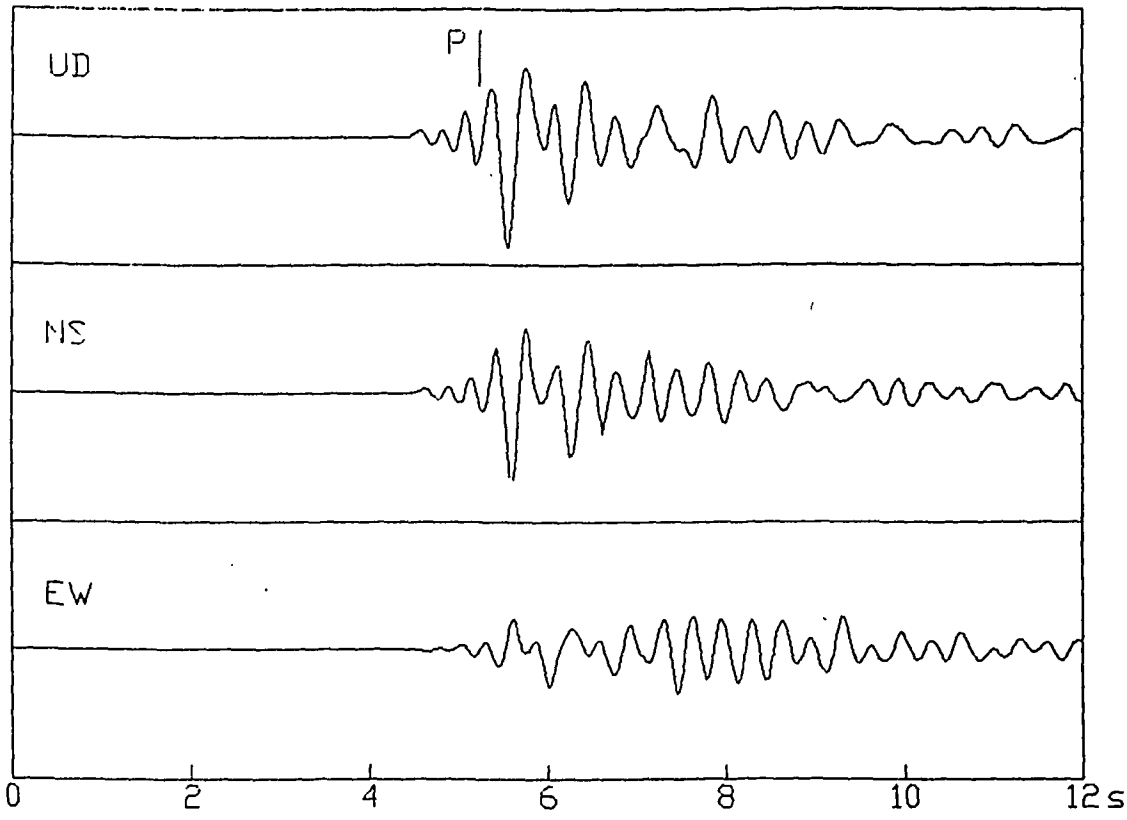

Fig.3a

Figure 3a Velocity seismogram from the Northern Japan Sea earthquake. In the figure the arrival of P-wave from the main event is indicated. For details see Kim and Lee (1995).

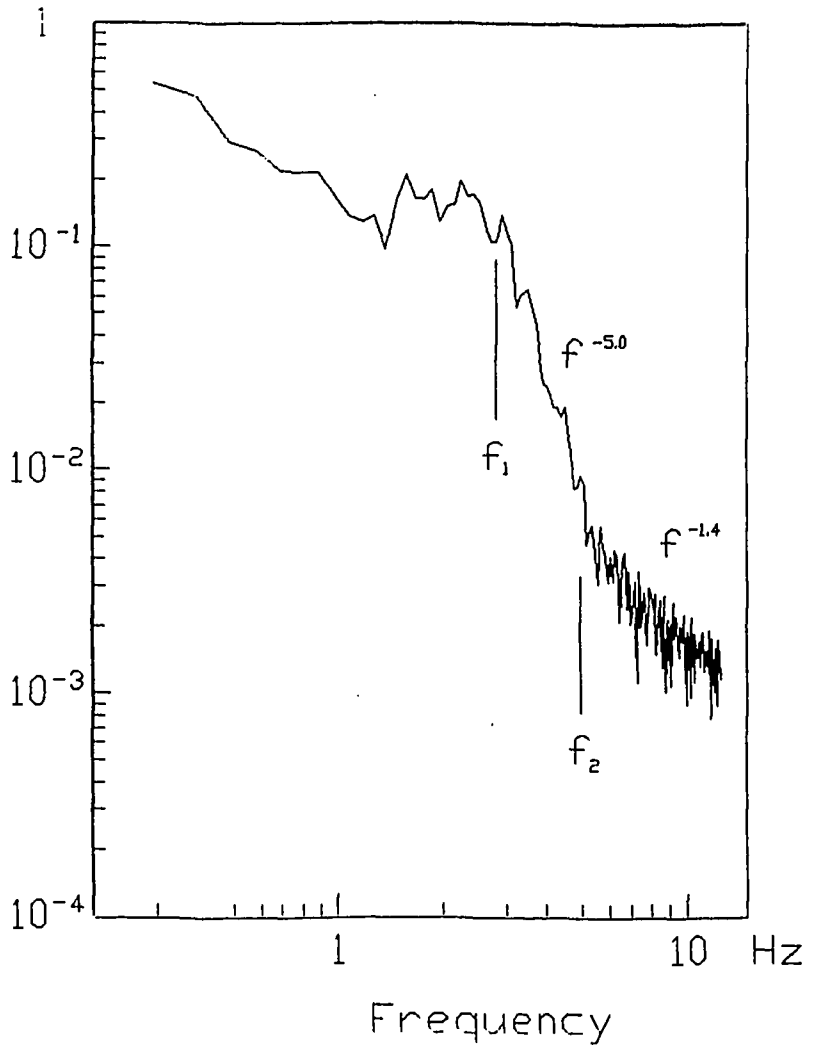

Fig.3b

Figure 3b Source spectra of the Northern Japan Sea earthquake. In the figure vertical axis is the relative amplitude. Corner frequencies are also indicated in the figure. See text for detail.